Effects of Navier–Stokes Characteristic Outflow Boundary Conditions : modeling for transverse flows

Eric Albin, Yves d'Angelo

Effects of Navier–Stokes Characteristic Outflow Boundary Conditions : modeling for transverse flows

E. Albin[1], Y. D'Angelo[2] *

[1] Post-doc, CNRS UMR6614 BP 12 76801 SAINT ETIENNE DU ROUVRAY, France
[2] Professor INSA Rouen, CORIA, CNRS UMR6614, BP 12 76801 SAINT ETIENNE DU ROUVRAY, France

Abstract
Navier–Stokes Characteristic Boundary Conditions are commonly used in DNS and LES to decrease the computational domain size and simulate practical engineering configurations. In this work, recent treatments of subsonic outflows are used and compared to evidence some limitations of these boundary conditions when the mainstream is transverse to the outflow. Some simulations of outgoing vortices and expanding premixed flames are performed to highlight the difficulties and distortions encountered with such transverse flows. A 3D-NSCBC-TOM outflow treatment is then proposed to reduce these distortions.

Introduction

Solving Navier-Stokes equations with compressible effects and non-periodic boundaries implies to deal with acoustic waves outgoing and ingoing into the computational domain. In the case of subsonic outflows with exiting velocities, most of the fluid information is computed from the inside of the domain but acoustic waves coming from the outside have to be modeled. Different models have been developed along years to damp the incoming acoustic waves.

In 1987, Thompson [1] prescribes the incoming characteristic wave amplitude by zero values to solve Euler equations. In 1992, Poinsot and Lele [2] extend this procedure to Navier-Stokes equations and introduce the so–called NSCBC treatment (for Navier-Stokes Characteristic Boundary Conditions). Their outflow treatment which assume the fluid to be locally inviscid, non reactive, and without transverse convective terms is known to generate strong spurious distortions [3]. Yoo *et al* [4, 3] include transverse, diffusive and reactive terms in the modeling of ingoing waves. Recently, Lodato *et al* [5] adapt this 3D-NSCBC strategy to Large Eddy Simulation (LES) [6] and introduce a particular treatment for edges and corners to avoid instabilities. This 3D-NSCBC treatment is known to drastically decrease flow distortions over previous treatments. It allows for instance to make a vortex going out normally to the boundary with a very few distortions even with temporary slightly negative velocities, to avoid the suction of a free jet towards edges, to keep the shape of an outgoing spherical pressure wave [6].

This 3D-NSCBC outflow treatment is used to compute turbulent expanding flames in large square or cubic domains. With such configurations, the flow is transverse to boundaries near edges and corners. Negative velocities can temporarily occur before the flame expansion makes vortices to go out from the computational domain. This first difficulty is discussed for both the cylindrical and the spherical turbulent expanding flame. Even with 3D-NSCBC outflows, it is shown that flames are becoming square. It is argued here that this outflow treatment does not describe a pertinent acceleration of the fluid when the mean flow is transverse to the boundary. A 3D-NSCBC-TOM model is proposed to improve the quantitative description of this acceleration.

* Corresponding author: dangelo@coria.fr
Proceedings of the European Combustion Meeting 2011

Outflow and inflow acoustic boundaries

To correctly solve a fluid flow problem, it is particularly important to accurately describe boundaries like inflows and outflows. In an open subsonic outflow boundary, the outside domain should not be a source of distortion for the inside flow field. The aim of present study is to highlight some remaining difficulties to correctly model the acoustic behavior from the outside. We show that some configurations like expanding flames can quickly lead to numerical difficulties because of outflow boundary conditions.

Expanding spherical flames are very common and can be analyzed through experiments [7, 8] or found in spark ignition engines. Simulating turbulent spherical expanding flames with DNS is useful to test some flame modeling approaches like the Evolution Equation Modeling (EEM) of [9] or LES subgrid models. Highly curved spherical flames can be observed, that may be very difficult to accurately measure experimentally because of spark ignition system. In the present work, we are mostly interested in the possibility to simulate large DNS of expanding flames, with the smallest computational domain. The use of recent improved outflow boundary condition is discussed since it has some importance both for the stability of the computation and the accuracy of the solution.

Expanding flames with 3D-NSCBC outflows

To solve large expanding flames, we use the numerical strategy described in [10] to reduce the effective CPU cost. The parallel code solves compressible NS equations with 6th order hybrid staggered-colocated explicit finite difference schemes and a third order Runge-Kutta time integration. Single step chemistry modeling is also used.

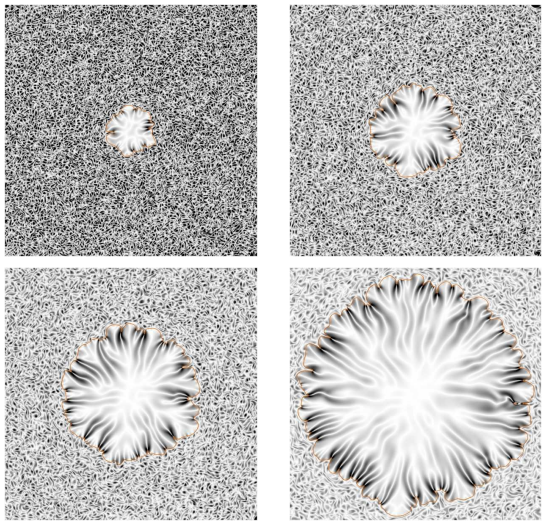

Figure 1: DNS of a cylindrical expanding flame in a $(20cm)^2$ square domain (Vorticity field in black gradient and iso-contours of reaction rate in color).

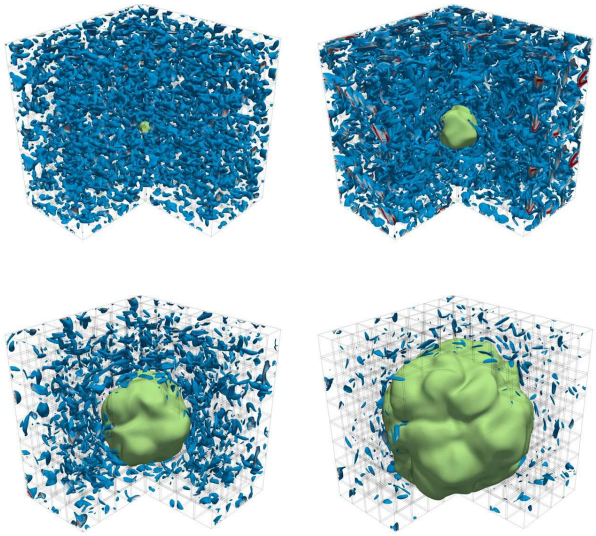

Figure 2: DNS of a spherical expanding flame in a $(3cm)^3$ cubic domain : iso-surfaces of vorticity (red to blue) and iso-surface of the reaction rate (in green).

A cylindrical expanding flame is solved in a two dimensional $(20cm)^2$ square box discretized by $(3200)^2$ nodes. The unburnt gas is a stoichiometric propane/air mixture ($S_L = 0.407m/s$, $Le = 1.4$). The initial turbulence is generated from a Passot-Pouquet spectrum with an integral scale $l_t = 3mm$ and a rms turbulent velocity $u'/S_L = 0.8$. The initial generic turbulence is first decreased with periodic boundary conditions to get a more realistic homogeneous isotropic turbulence. Periodic boundaries are then replaced by 3D-NSCBC outflow boundaries of Yoo *et* Im [3] and the mixture is ignited by a very localized Gaussian temperature profile. Details about this initialization can be found in [11]. The flame evolution is then solved for a physical time of $29ms$. Contours of reaction rates and vorticity fields are plotted figure 1, respectively at times $t = 7.2$, 12, 16.8 and $26.4ms$ after the ignition.

A 3D spherical expanding flame is solved in a $(3cm)^3$ cubic box discretized with $(480)^3$ nodes. The unburnt gas are a stoichiometric propane/air pre-mixture and the turbulence has the same initial properties than in the previous case. The same procedure is applied to get an homogeneous isotropic turbulence, and then ignite the mixture. The flame dynamics are solved during $7.28ms$. Figure 2 plots some reaction rate and vorticity isosurfaces at times $t = 0.49$, 2.43, 4.37 and $6.31ms$. This computation required 120 hours using 512 processors (i.e. around 61000 CPU hours) while the previous 2D cylindrical flame approximately required 60 hours with 256 processes at 4.7GHz.

The time evolution of the vorticity field in Fig. 1 shows that turbulence decreases in time and also that the vortex size increases. It may also be noticed the vorticity increase at the right corners of the computational domain ; this is particularly visible between the first and the second picture. Nevertheless, 3D-NSCBC outflows allow temporary negative velocities as it has been observed with a vortex test-case in [6]. Gas expansion through the flame acts as a piston that pushes the fresh mixture outside from the computational domain. It may be observed on the third and fourth pictures than the unphysical increase of viscosity near the corners have disappeared. This means the flame expansion is sufficient in this case to counterbalance the temporary negative velocities due to vortices. In the case of the spherical expanding flame, we however encountered some oscillations that appeared at the outflows and generated negative temperatures at $t = 3.16ms$, hence stopped the computation. The unphysical increase of vorticity can be visualized on the second picture of Fig. 2 ($t = 2.43ms$). Indeed, the red iso-surfaces are much more present at the boundaries than inside the vortical structures located on the two inside planes. The physical viscosity has then been artificially multiplied by a factor of 3 at less than $2mm$ from the outflows to avoid these oscillations. This artificial patch at boundaries has only been used for a short time compared to the length of the simulation and it has only been necessary in this turbulent 3D expanding case at early times.

In order to explain why the turbulent 3D case is numerically more unstable and hard to compute, we performed DNS of planar, cylindrical and spherical laminar stoichiometric propane/air flame respectively, in a 1D, 2D and 3D plane-parallel domain.

For each of these cases, a vector $\overrightarrow{e_r}$ normal to the flame front is defined. The distance r_f represents the radius of the flame front for the cylindrical and spherical case and is the distance between flame fronts and the symmetry plan in the planar case. For $|r| > r_f$ gases are

unburnt and they are burnt inside the flame. Because of the symmetry of such laminar flames, all velocities depend only on r. They are directed along $\overrightarrow{e_r}$ and the velocity is zero for $r = 0$. During a small time-step dt, the variation of unburnt gases is $dm_u = -\rho_u dV_u$ with $dV_u = SS_c dt$, S being the flame front surface and S_c the consumption speed of unburnt gases. In these expanding flames, the variation of burnt gases is $dm_b = \rho_b dV_b$ with $dV_b = Sdr_f$ (spherical case : $d(4\pi r_f^3/3) = Sdr_f$). For the planar, the cylindrical and the spherical case, the conservation of mass through the interface implies

$$v_{f/\emptyset} = \frac{dr_f}{dt} = \frac{S_c}{1-\alpha} \tag{1}$$

where $\alpha = (\rho_u - \rho_b)/\rho_u = (T_b - T_u)/T_b = 0.85$ is the dilatation coefficient and $v_{f/\emptyset}$ is the flame velocity relative to a fixed referential denoted $\emptyset$. It is well known that the consumption velocity depends on flame stretch $\kappa = 1/S \cdot dS/dt = \frac{a}{r_f}\frac{dr_f}{dt}$ (a=0, 1 and 2 for the planar, the cylindrical and the spherical current expanding flame). This phenomenon is usually [8] represented by Markstein's law (2) where $\mathcal{L}$ is the Markstein length. Note this stretch effect could be inverted for some mixtures like lean hydrogen/air where thermodiffusive properties are different ($Le < 1$).

$$S_c = S_L - (1-\alpha)\mathcal{L}\cdot\kappa = S_L \cdot \frac{1}{1+\mathcal{L}\cdot\frac{a}{r_f}} \tag{2}$$

Figure 3 compares flame velocity against flame radius, as predicted by Markstein's laws ($\mathcal{L} = 657\mu m$ in the cylindrical case and $\mathcal{L} = 920\mu m$ in the spherical case), DNS (in 3D and 2D cylindrical). These numerical/theoretical results are compared to measurements by Lecordier [7] on real stoichiometric atmospheric propane-air spherical flames. Note that the 3D DNS compares well with both Markstein's theory and experimental data. High spatio-temporal refinement of the DNS allows to accurately compute flame radius evolution at small radii, which is not the case in the experimental measurements.

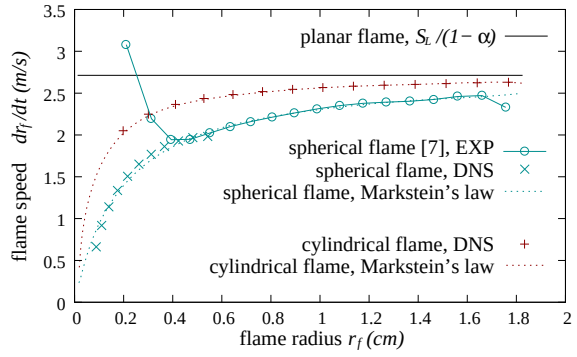

Figure 3: Evolution of flame speed for a planar, a cylindrical and a spherical stoichiometric propane-air flame. Comparison between DNS, Lecordier's experiment [7] and Markstein's theory.

At small scale, the ignition system (here a spark) does not allow for accurate measurements. On the other hand, DNS is not able to provide results at large radii because the computational size of the domain is limited. The 2D cylindrical DNS is also compatible with Markstein's law but with a different Markstein length [12]. This Markstein length does not appear to be a universal constant depending only on the mixture since it also depends on flame configuration. For a given radius, the spherical flame speed is smaller than the cylindrical flame speed. In this case, both flame curvature and Markstein's length are larger (cf. equation 2). This makes the spherical flame piston effect less efficient to push vortices outside the computational domain.

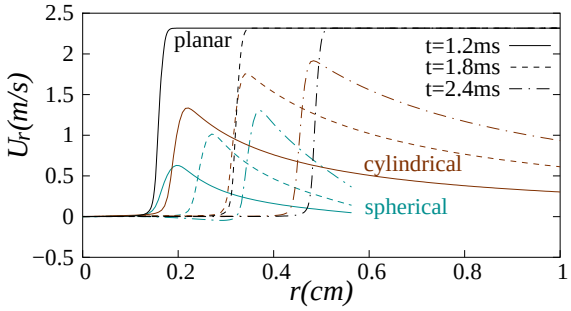

Figure 4: DNS results showing the U_r velocities of gases along the $(O, \vec{e}_r)$ axis for a planar, a cylindrical and a spherical expanding flame.

However, these variations of the consumption speed are not the only reason decreasing this piston effect. Figure 4 plots gas velocity along the $(O, \overrightarrow{e_r})$ axis for three basic geometrical configurations of expanding flames. These velocity profiles are plotted at three different times to visualize velocity time evolution. If one defines the velocity of unburnt gas relative to the referential attached to the flame and just at the flame by $v_{u/f} = -S_c$, the absolute velocity of unburnt gas is

$$v_{u/\emptyset}(r_f) = v_{u/b} = \frac{\alpha}{1-\alpha}S_c \tag{3}$$

In the planar case, because of gas expansion, this velocity jump (3) is quite larger than the laminar flame speed S_L, as it may be visualized on Fig. 4. This jump is much weaker for the cylindrical and spherical cases because of the geometrical change of volume and of the curvature/stretch effect on the front, as previously described. Fig. 4 also shows that unburnt gas velocity decreases much faster (in space) for the spherical case. This can be easily understood by a geometrical argument. If R denotes a distance $r = R > r_f$, let define a control volume containing a given quantity of (unburnt and burnt) gas. The volumes of unburnt and burnt gas contained in this control volume at time t are respectively denoted by V_u^t and V_b^t. The respective volumes of burnt and of unburnt gas inside this control volume are related by

$$V_{u+b}^{t+dt} = V_u^t + V_b^t + \underbrace{dV_u + dV_b}_{\frac{\alpha}{1-\alpha}S\cdot S_c dt} \tag{4}$$

with dV_u and dV_b the variation of burnt and unburnt mixture. Since this control volume is following the unburnt gas at its boundary, the variation of volume are still $dV_u = -S \cdot S_c dt$ and $dV_b = dV_u/(1-\alpha)$. The control volume depends on geometry:

$$V^t_{u+b} = \frac{SR^{a+1}}{(a+1)\cdot r_f^a} \tag{5}$$

with respectively $a = 0$, 1 or 2 for planar, cylindrical or spherical geometry. Replacing the control volume expression (5) in the volume conservation equation (4), the velocity of unburnt gas is straightforwardly expressed by equation (6) as a function of radius R, flame radius r_f, geometry coefficient a and consumption speed S_c.

$$v_{u/\emptyset}(R \geq r_f) = \frac{dR}{dt} = \frac{\alpha}{1-\alpha}\left(\frac{r_f}{R}\right)^a S_c \tag{6}$$

Since the velocity field has only one component, depending only on spatial coordinate R, the unburnt zone is incompressible (div $\overrightarrow{v_{u/\emptyset}} = 1/R^a \cdot \partial R^a v_{u/\emptyset}/\partial R = 0$). Equation (3) is recovered for $R = r_f$. While all unburnt gases are pushed as a whole with constant velocity in the planar case, this velocity quickly decreases near the flame front for the cylindrical and spherical expanding flames ; it decreases respectively in $\mathcal{O}(R)$ and $\mathcal{O}(R^2)$. This fast spatial decrease of the unburnt velocity is the main reason explaining why turbulent 3D expanding flames are more difficult to compute. In the spherical case, unburnt gases are hardly pushed by the active interface because of the low consumption speed and of this fast spatial decrease of velocity near the flame. Hence, with no special treatment at the outflows, the initial turbulent flow can induce local inflow at the outlets, possibly yielding numerical instabilities (as it will be evoked next section).

For a moderate level of turbulence intensity $u'/S_L = 0.8$, a $(20cm)^2$ 2D computation does not face any stability problem while a $(3cm)^3$ 3D simulation must cope with possible negative velocities at boundaries.

Another important boundary effect is that 3D-NSCBC outflows make the cylindrical flame to be slightly square shaped [3]. For the 3D calculation, this squared shape is visible on fourth picture of Fig. 1 and patent in figure 5. This behavior is still present in $3D$ when the spherical interface approaches outflows (see PhD [11]). One may also notice the small negative velocities appearing in burnt gases at $t = 2.4ms$ for the spherical case. This is an effect of 3D NSCBC treatment. In the second part of the discussion (next section) we shall try and explain this behavior. We shall also propose and present a strategy to correct it.

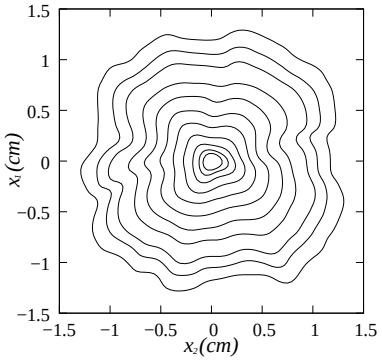

Figure 5: A planar cut of the 3D calculation of figure 2, with 3D NSCBC outflows. The flame tends to adopt a squared shape when approaching boundaries.

2. 3D-NSCBC-TOM outflows :

We attribute the squared shapes observed on previous flame tests to the effect of boundary condition. Indeed, we think that 3D-NSCBC outflow treatment do not pertinently model the correct acceleration of the fluid flow when the mainstream is transverse to the boundary. To evidence distortions generated by this 3D-NSCBC outflow treatment, a modified treatment of acoustic waves at outflow boundaries is proposed in [11], to be able to deal with transverse flows. For the sake of brevity, full details of this proposed 3D-NSCBC-TOM (Transverse Outflow Modified) outflow treatment are not presented here. More details can however be found in [11] and [13]. Below we shall only present the outline of the proposed strategy.

The characteristic wave decomposition, that comes from a rigorous mathematical development, does not depend on the chosen referential. Characteristic waves may be for instance decomposed on a referential $\widehat{\mathcal{R}}$ based on the outgoing normal $\overrightarrow{\widehat{x}_1}$ of the computational domain and it could also be decomposed on a referential $\widetilde{\mathcal{R}}$ based on the local velocity $\overrightarrow{U} = U \cdot \overrightarrow{\widetilde{x}_1}$. Figure 6 plots characteristic velocities of acoustic waves for these two referentials. In referential $\widehat{\mathcal{R}}$, $\widehat{\mathcal{L}}^i_4$ and $\widehat{\mathcal{L}}^i_5$ advective terms are respectively propagating acoustic characteristics with component velocities $\widehat{U}_i - c$ and $\widehat{U}_i + c$ ($i \in \{1;2\}$). In the referential $\widetilde{\mathcal{R}}$, $\widetilde{\mathcal{L}}^1_{4\&5}$ terms are propagating acoustic characterics with velocities $\widetilde{U}_i \pm c$ and $\widetilde{\mathcal{L}}^2_{4\&5}$ with $\pm c$ velocities since $\widetilde{U}_2 = 0$. With some mathematical developments, it is possible to show that the acceleration $\rho \partial \overrightarrow{U}/\partial t$ does not

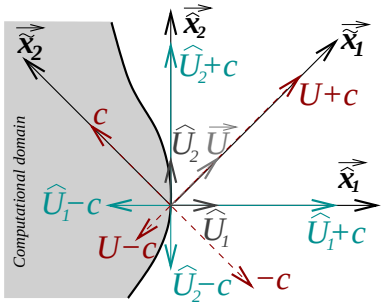

Figure 6: Schematic representation of characteristic velocities along a referential $\widehat{\mathcal{R}}$ based on the outflow geometry or along a referential $\widetilde{\mathcal{R}}$ based on the local velocity $\vec{U}$; c is the sound velocity.

depend on the choice of a referential because of its rotational invariances. Equation (7) express the fact that fluid acceleration decomposed on the geometrical frame $\widehat{\mathcal{R}}$ is rigorously the same than the acceleration decomposed on the streamline based frame $\widetilde{\mathcal{R}}$.

$$\rho\left(\frac{\partial\widetilde{U}_1}{\partial t}\widetilde{\mathbf{x}}_1+\frac{\partial\widetilde{U}_2}{\partial t}\widetilde{\mathbf{x}}_2\right)=\rho\left(\frac{\partial\widehat{U}_1}{\partial t}\widehat{\mathbf{x}}_1+\frac{\partial\widehat{U}_2}{\partial t}\widehat{\mathbf{x}}_2\right) \quad (7)$$

This equation is verified when all $\mathcal{L}^i_{4\&5}$ advective terms may be computed by their analytical expressions. However, whenever $\widehat{\mathcal{L}}^1_4$ or $\widetilde{\mathcal{L}}^1_4$ incoming advective terms are modeled, this equation can only be approximately true.

With 3D-NSCBC outflows, the incoming advective term $\widehat{\mathcal{L}}^1_4$ is prescribed with a transverse relaxation coefficient. This relaxation coefficient comes from an asymptotic analysis of Yoo *et* Im [3] which supposes the mean flow to be one-directional ($\widetilde{U}_2 \simeq 0$), e.g. for an analysis in the streamline based referential $\widetilde{\mathcal{R}}$. The use of this coefficient in the $\widehat{\mathcal{R}}$ geometrical referential is not straightforward since it has been noticed that the flow acceleration depends on the considered referential as soon as one amplitude $\widehat{\mathcal{L}}^1_4$ is modeled. In the tested 3D-NSCBC-TOM strategy, $\widetilde{\mathcal{L}}^1_4$ is prescribed by a 3D-NSCBC outflow treatment in accordance with the asymptotic analysis of Yoo. The 3D-NSCBC-TOM strategy can then be viewed as a collection of 3D-NSCBC outflows dynamically oriented along the streamlines.

A first test of 3D-NSCBC-TOM outflows is presented in figure 7. A vortex is convected towards the upright corner with a Ma=0.2 horizontal and vertical Mach number ; the counter-clock vortex has only a maximum orthoradial velocity characterized by Ma=0.006. This simulation is performed both with 3D-NSCBC outflows and with 3D-NSCBC-TOM outflows. Iso-contours of vorticity and density field are plotted at times $t = 19, 56$ and 93 μs for these two different boundary treatments. Strong distortions of the vortex may be observed on figure 7a with 3D-NSCBC outflows ; these distortions are considerably reduced on figure 7b with 3D-NSCBC-TOM outflow treatment. This evidences that the flow acceleration is not pertinently modeled with 3D-NSCBC outflows when the mainstream is not normal to the boundary. With 3D-NSCBC-TOM outflows, this flow acceleration is predicted in accordance with the asymptotic analyses of Yoo *et* Im [3] which supposes the flow locally unidirectional.

A second test of 3D-NSCBC-TOM outflows is presented in figure 8. A stoichiometric methane/air mixture is ignited with a Gaussian temperature profile, in a $(2.4cm)^2$ square box. One simulation is performed with four 3D-NSCBC outflows and another with four 3D-NSCBC-TOM outflows. Fig. 8 plots the vector velocity field and the density at time $t = 385\mu s$ in one fourth of the computational domain. One may notice that the velocity field is not the same at boundaries when comparing figure 8a to 8b. With 3D-NSCBC outflows, the flame is too fast-flowing near the corner, when flow is transverse to the boundary. The non-pertinent flow acceleration makes the flame to get a square shape with 3D-NSCBC treatment, which is not the case with the 3D-NSCBC-TOM strategy. However, 3D-NSCBC-TOM treatment may be not sufficiently robust for not so well de-

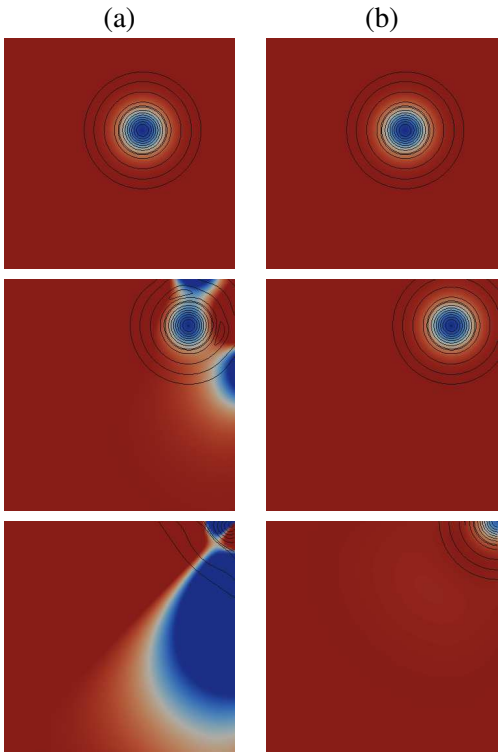

Figure 7: Outgoing vortex at upright corner for two different outflow treatments. Iso-contours of vorticity in black and density field in color.

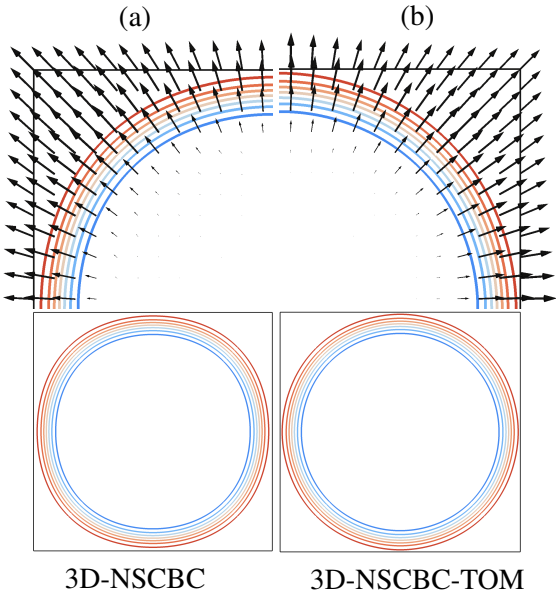

Figure 8: Laminar cylindrical expanding flame for two different treatments of open boundaries. Vector velocities in black, iso-contours of density in color.

fined outflows. As all outflow treatments should, it absolutely does not allow for negative outflowing velocity since $\mathcal{R}$ is defined from the outgoing velocity. Note that in the 4th picture of Fig. 1, the squared shape of the turbulent flame does not seem to be accelerated but decelerated near corners. In this particular turbulent case, temporary negative velocities at corners are amplified before expansion of the flame makes them go ; these boundary disturbances are therefore believed to affect the flame geometry.

Conclusions

The simulation of a large cylindrical and spherical expanding flame in a moderate turbulence has shown that the obtained solution strongly depends on open boundary conditions. Temporary negative velocities which are pushed out from the computational domain by the flame expansion have been shown to generate some instabilities with 3D-NSCBC outflows. These instabilities have been particularly difficult to handle in the spherical case for several reasons. The high curvature and the high measured Markstein's length of the spherical flame has first been shown to decelerate the consumption speed and then to decrease the flame expansion compared to a cylindrical expansion. Unburnt gas velocities which decrease much faster in the spherical case also makes the piston effect of the flame less efficient. A vortex simulation and a laminar cylindrical expanding flame have evidenced that 3D-NSCBC outflows do not perfectly model the flow acceleration at boundaries and may square expanding flames. The 3D-NSCBC-TOM proposed strategy has shown the reason of these boundary distortions. This treatment demonstrates that it is possible to accurately prescribe the fluid acceleration at open boundaries when modeling the acoustic effect of the outside. However, further developments are still required, in order to use this strategy in engineering situations.

Acknowledgements

This work was granted access to the HPC resources of CRIHAN and also IDRIS under the allocation 2010-026186 made by GENCI.

References

[1] K. Thompson, Time-dependent boundary conditions for hyperbolic systems I, Journal of Computational Physics 68 (1987) 1–24.

[2] T. Poinsot, S. Lele, Boundary conditions for direct simulations of compressible viscous flows, Journal of computational physics 101 (1) (1992) 104–129.

[3] C. S. Yoo, H. G. Im, Characteristic boundary conditions for simulations of compressible reacting flows with multi-dimensional, viscous and reaction effects, Combustion Theory and Modelling 11 (2) (2007) 259–286.

[4] C. Yoo, Y. Wang, A. Trouvé, H. Im, Characteristic boundary conditions for direct simulations of turbulent counterflow flames, Combustion Theory and Modelling 9 (4) (2005) 617–646.

[5] G. Lodato, P. Domingo, L. Vervisch, Three-dimensional boundary conditions for direct and large-eddy simulation of compressible viscous flows, Journal of Computational Physics 227 (10) (2008) 5105–5143.

[6] G. Lodato, L. Vervisch, P. Domingo, A compresssible wall-adapting similarity mixed model for large-eddy simulation of the impinging round jet, Phys. Fluids 21 (2009) 035102.

[7] B. Lecordier, Etude de l'interaction de la propagation d'une flamme prémélangée avec le champ aérodynamique par association de la tomographie laser et de la PIV, PhD thesis.

[8] B. Renou, A. Boukhalfa, D. Puechberty, M. Trinité, Local scalar flame properties of freely propagating premixed turbulent flames at various Lewis numbers, Combustion and Flame 123 (4) (2000) 507–521.

[9] Y. D'Angelo, G. Joulin, G. Boury, On model evolution equations for the whole surface of three-dimensional expanding wrinkled premixed flames, Combustion Theory and Modelling 4 (3) (2000) 317–338.

[10] E. Albin, Y. D'Angelo, L. Vervisch, Using staggered grids with characteristic boundary conditions when solving compressible reactive Navier–Stokes equations, International Journal for Numerical Methods in Fluids (2010) .

[11] E. Albin, Contribution à la modélisation numérique des flammes turbulentes : comparaisons DNS-EEM-Expériences., PhD thesis (2010) .

[12] D. Durox, S. Ducruix, S. Candel, Experiments on collapsing cylindrical flames, Combustion and Flame 125 (1-2) (2001) 982–1000.

[13] E. Albin, Y. D'Angelo, L. Vervisch, Flow streamline based Navier–Stokes characteristic boundary conditions : modeling for transverse and corner outflows, Computers & Fluids (2011) .